Fatigue Damage Estimation and Data-based Control for Wind Turbines

Barradas Berglind, Jose de Jesus; Wisniewski, Rafal; Soltani, Mohsen

Published in:
IET Control Theory & Applications

DOI (link to publication from Publisher):
10.1049/iet-cta.2014.0730

Publication date:
2015

Document Version
Accepted author manuscript, peer reviewed version

Published in IET Control Theory and Applications
Received on 29th June 2014
Revised on 3rd October 2014
Accepted on 21st November 2014
doi: 10.1049/iet-cta.2014.0730

ISSN 1751-8644

Fatigue damage estimation and data-based control for wind turbines

Jose de Jesus Barradas-Berglind[1], *Rafael Wisniewski*[1], *Mohsen Soltani*[2]

[1] *Department of Electronic Systems, Aalborg University, Aalborg East 9220, Denmark*
[2] *Department of Energy Technology, Aalborg University, Esbjerg 6700, Denmark*
E-mail: jjb@es.aau.dk

Abstract: The focus of this work is on fatigue estimation and data-based controller design for wind turbines. The main purpose is to include a model of the fatigue damage of the wind turbine components in the controller design and synthesis process. This study addresses an online fatigue estimation method based on hysteresis operators, which can be used in control loops. The authors propose a data-based model predictive control (MPC) strategy that incorporates an online fatigue estimation method through the objective function, where the ultimate goal in mind is to reduce the fatigue damage of the wind turbine components. The outcome is an adaptive or self-tuning MPC strategy for wind turbine fatigue damage reduction, which relies on parameter identification on previous measurement data. The results of the proposed strategy are compared with a baseline model predictive controller.

1 Introduction

Fatigue damage in general terms can be understood as the weakening or breakdown of a material subject to stress, especially a repeated series of stresses. From a materials perspective, it can be also thought as the (elastoplastic) deformations that cause damage on a certain material or structure, compromising its integrity as a result. In other words, fatigue is a phenomenon that occurs in a microscopic scale, manifesting itself as deterioration or damage in components or structures. Due to this fact, it has been of great interest in different fields and has been extensively studied with different perspectives; a very detailed history of fatigue can be found in [1]. It could be argued that two major turning points on the history of fatigue came firstly with the contributions of Wöhler, who as early as 1860 suggested design for the finite fatigue life [2] and the so-called Wöhler curve (or S-N curve stress against number of cycles to failure); and secondly, with the linear damage accumulation rule by Palmgren [3] and Miner [4], which is still the basis for theoretical damage estimation.

Fatigue is generally estimated using the rainflow counting (RFC) method first introduced by Endo *et al.* [5], which is used in combination with the aforementioned Palgrem–Miner rule of linear damage accumulation. The motivation for this work is to facilitate the shortcomings of the RFC method, which has an algorithmic non-linear structure, requiring deletions as well as a significant history window, and thus used mainly as a post-processing tool. In the wind turbine control context, current control methods are based on minimisation of certain norms of the stress on different components of the wind turbine, which are expected to reduce fatigue, but are not a reliable characterisation of the damage [6, 7]. Other approaches, such as taking the variance of a stress are not a direct representation of fatigue, as mentioned in [8]. In [9–11], loading reductions are achieved by controlling the pitch of each blade independently, but the damage is estimated offline. In [8], controllers for wind turbines were designed by approximating fatigue load by an analytical function based on spectral moments, where it is assumed that the stress is an output from a given linear system with Gaussian white noise input, but measurements are not directly used. In the wind farm level [12] presents a control algorithm, which aims at optimising power production and reducing structural loads.

In [13], an equivalence between symmetric RFC and a particular hysteresis operator is provided, allowing to incorporate a fatigue estimator online within the control loop. In this paper, we propose a data-driven control scheme that approximates the fatigue loads provided by such a hysteresis operator, which is consistent with the model predictive control (MPC) formalism. Optimal control problems with hysteresis were studied in [14] using necessary conditions for Pontryagin's extremum principle. In [15], the dynamic programming equations for controlled differential equations with hysteresis on the control input were introduced and in [16], optimisation problems for controlled dynamical systems in discrete time with Preisach hysteresis are considered. In the framework of viscosity solutions of the Hamilton–Jacobi–Bellman equation, the optimal control problem was addressed for a weighted sum of delayed relays in [17] and for systems with Preisach hysteresis in [18]. Despite the theoretical soundness of the previous results, their applicability to control of complex physical systems is limited by computational tractability. To overcome this disadvantage, our approach provides tuning parameters to the controller,

which can be comparable to iterative feedback tuning (IFT) techniques [19, 20], where the controller is refined iteratively. In [20, 21], comprehensive overviews of data-based techniques focused on modern large-scale industrial applications are presented. Recent developments in data-based techniques have been presented in [22–24] for fault detection and diagnosis.

The contributions of the present work are three-fold: (i) to bring attention to a fatigue damage estimation method based on hysteresis operators that can be implemented online for control purposes; (ii) to propose a least squares approximation technique of the aforementioned damage estimation based on the shaft torsion and its first derivative; and (iii) to introduce a self-tuning data-based MPC strategy for wind turbine fatigue damage reduction. The intention of this paper is to consider the incurred damage to the turbine components introduced by operating varying wind loading. Accordingly, the data-driven approach taken on this paper provides an estimated fatigue model which: (A) can be used in real-time control and is not limited by computational power and (B) gives a closed mathematical formulation of fatigue which can be used in control design and optimisation.

The remainder of this paper is organised as follows: Section 2 elaborates on the fatigue damage estimation; in Section 3 the hysteresis method is introduced, together with some properties of a particular hysteresis operator in Section 4. Subsequently, Section 5 elaborates on the wind turbine model to be used and Section 6 presents the proposed fatigue damage reduction control strategy. Lastly, simulation results and conclusions are presented in Sections 7 and 8, respectively.

2 Fatigue damage estimation

Perhaps the most recognised and used measure of fatigue is the so-called rainflow counting method. First introduced by Endo *et al.* [5], it has a complex sequential structure in order to decompose arbitrary sequences of loads into cycles; its name comes from an analogy with roofs collecting rainwater, used to explain the algorithm. Typically, to compute a lifetime estimate from a given structural stress input, the RFC method is applied by counting cycles and extrema, followed by the Palmgren–Miner rule [3, 4] together with the material-specific S-N coefficients to calculate the expected damage; a figure depicting the RFC method is shown in Fig. 1. Often, load signals are discretised to a certain number of levels, allowing an efficient storage of the cycles in a so-called rainflow matrix that is an upper triangular matrix by definition (see [25] for details). There are many equivalent descriptions of the RFC method, such as the ones in [26, 27]. From an implementation perspective, Niesłony [28] developed a toolbox to perform the RFC algorithm. Nevertheless, the RFC method is a very non-linear numerical algorithm and not a mathematical function; thus it can only be used as a post-processing algorithm, or in other words it is always performed offline. Hence, it is not possible to use RFC for real-time control, since it requires a time series of stress and not only instantaneous measurements, as it is the case in control loops.

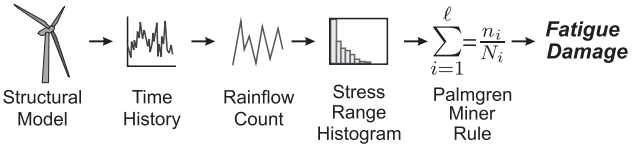

Fig. 1 *RFC damage estimation procedure*

Alternatives to the RFC method include the usage of stochastic processes [29] and the so-called frequency domain approximations or spectral methods [30]. An energy based approach to fatigue is taken in [31], where an incremental method for the calculation of dissipated energy under random loading is presented, and the dissipated hysteresis energy to failure is used as the fatigue life parameter. This notion has a strong physical meaning, since an amount of energy is dissipated, as damage is introduced to a material or structure. As mentioned in [26], the purpose of the RFC method is precisely to identify the closed hysteresis loops in the stress and strain signals.

In [13], an equivalence between the symmetric RFC and a particular hysteresis operator is provided. The latter approach has the advantage that it can be incorporated online in the control loop, in contrast to the RFC method. An additional advantage is that the hysteresis method is closely related to the physical behaviour of the damaging process, which will be further discussed in the following section.

3 Damage calculation via hysteresis operators

As explained in [13], if one associates values to individual cycles or hysteresis loops, one assumes that the underlying process is rate independent. The previous implies that only the hysteresis loops themselves are important, but not the speed with which they are traversed; in the case of damage, it does not matter how fast the stress occurs, but its magnitude. Rate independent processes are mathematically formalised as hysteresis operators, for details see [32–34].

Firstly, the notion of string is introduced as a way to represent the stresses for damage calculation.

Definition 1 (string): Let $s = (v_0, \ldots, v_N) \in S$ be a given string, which represents an arbitrary load sequence.

1. Let S be the space of finite sequences in $\mathbb{R}$, that is, $S = \{(v_0, v_1, \ldots, v_N) : N \in \mathbb{N}_0, v_i \in \mathbb{R}, 0 \leq i \leq N\}$, $\mathbb{N}_0 = \mathbb{N} \cup \{0\}$.
2. Denote the concatenation of two strings $s = (v_0, \ldots, v_N)$ and $s' = (v'_0, \ldots, v'_N)$ by $(s, s') = (v_0, \ldots, v_N, v'_0, \ldots, v'_N)$.

Following the interpretation of RFC given in [34], we introduce $N(\mu, \tau)$ with values μ and τ, chosen such that the input string $s = (v_0, \ldots, v_N)$ with $v_{2k} = \mu$ and $v_{2k+1} = \tau$ for $k \in \mathbb{N}_0$, destroys the specimen after $N(\mu, \tau) = \tilde{N}(|\tau - \mu|)$ cycles; the resulting curve is the so called Wöhler or S-N curve, since the ansatz

$$\tilde{N}(\mu, \tau) = \kappa_1 |\mu - \tau|^{\kappa_2} \tag{1}$$

exhibits a straight line in a log-log scale, where κ_1 and κ_2 are scaling constants and $|\mu - \tau|$ is a given stress range. Subsequently, the Palmgren–Miner rule is used to identify and count cycles for an arbitrary stress $s \in S$, such that the damage accumulation is obtained as

$$D_{\text{ac}}(s) := \sum_{\mu < \tau} \frac{c(s)(\mu, \tau)}{N(\mu, \tau)} \tag{2}$$

doi: 10.1049/iet-cta.2014.0730

where $c(s)(\mu,\tau)$ is the rainflow count associated with a fixed s. The damage accumulation rule can be redefined considering a periodic rainflow count $c_{\text{per}}(s) := c(s) + c(s_{\mathcal{M}}, s_{\mathcal{M}})$ as

$$D_{\text{ac}}(s) := \sum_{\mu<\tau} \frac{c_{\text{per}}(s)(\mu,\tau)}{N(\mu,\tau)} \tag{3}$$

in order to take into account the contribution of the residual $s_{\mathcal{M}}$ (see the Appendix for details).

Before presenting the equivalence between RFC and the hysteresis method, the basic relay operator, variation and Preisach hysteresis operators will be introduced.

Definition 2 (relay hysteresis operator): Let $\mu, \tau \in \mathbb{R}$ with $\mu < \tau$ and $w_{-1} \in \{0, 1\}$ be given. We define the relay operator $\mathcal{R}_{\mu,\tau} : S \to S$ by

$$\mathcal{R}_{\mu,\tau}(v_0, \ldots, v_N) = (w_0, \ldots, w_N) \tag{4}$$

with

$$w_i = \begin{cases} 1, & v_i \geq \tau \\ 0, & v_i \leq \mu \\ w_{i-1}, & \mu < v_i < \tau \end{cases} \tag{5}$$

Definition 3 (variation): For any string $s = (v_0, \ldots, v_N) \in S$, we define its variation $\text{Var} : s \to \mathbb{R}$ by

$$\text{Var}(s) = \sum_{i=0}^{N-1} |v_{i+1} - v_i| \tag{6}$$

Within the context of fatigue analysis, there is no reason to consider arbitrarily large input values. The relevant threshold values for the relays $\mathcal{R}_{\mu,\tau}$ then lie within the triangle

$$P = \left\{(\mu,\tau) \in \mathbb{R}^2, -M \leq \mu \leq \tau \leq M\right\} \tag{7}$$

known as the Preisach plane, where M is an a priori bound for admissible input values.

Definition 4 (Preisach hysteresis operator): Let the density function $\rho(\mu,\tau)$ be given. We define the Preisach operator $\mathcal{W} : S \to S$ as

$$\mathcal{W}(s) = \int_{\mu<\tau} \rho(\mu,\tau)\mathcal{R}_{\mu,\tau}(s)\,\mathrm{d}\mu\,\mathrm{d}\tau \tag{8}$$

Here, the integral is understood to be component-wise with respect to the elements of the string $\mathcal{R}_{\mu,\tau}(s)$ and the function ρ is set to zero outside the triangle P (or more formally stated as ρ having compact support).

The core result we lean on is the equivalence provided in [13, 34] between symmetric RFC and a Preisach hysteresis operator (first introduced in [35]), which is given as follows:

Proposition 5 (damage equivalence): Let $\mathcal{W}^{\text{per}}(s)$ be the periodic version of the Preisach operator with density function $\rho(\mu,\tau)$, such that for each sequence of stresses $s = (v_0, \ldots, v_N) \in S$ with $\|s\|_\infty \leq M$ and $v_0 = v_N$ the total damage $D_{\text{ac}}(s)$ associated to s satisfies

$$D_{\text{ac}}(s) = \sum_{\mu<\tau} \frac{c_{\text{per}}(s)(\mu,\tau)}{N(\mu,\tau)} = \text{Var}(\mathcal{W}^{\text{per}}(s)) \tag{9}$$

The left-hand side of the equivalence in (9) corresponds to the symmetric RFC, such that $N(\mu,\tau)$ denotes the number of times a repetition of the input cycle (μ,τ) leads to failure. The right-hand side of (9) corresponds to

$$\text{Var}(\mathcal{W}^{\text{per}}(s)) = \int_{\mu<\tau} \rho(\mu,\tau)\text{Var}(\mathcal{R}^{\text{per}}_{\mu,\tau}(s))\,\mathrm{d}\mu\,\mathrm{d}\tau \tag{10}$$

where its density function ρ is a function of $N(\mu,\tau)$ and $\mathcal{R}^{\text{per}}_{\mu,\tau}$ is the periodic version of the relay operator $\mathcal{R}_{\mu,\tau}$, such that the equivalence also contains the residual (for details regarding these periodic operators see the Appendix). For details on the previous refer to Theorem 2.12.6 and Corollary 2.12.7 in [34]. The interpretation of the previous result is that the RFC method counts the number of oscillations at each range of amplitude, and this is precisely what the value $\text{Var}(\mathcal{W}^{\text{per}}(s))$ represents, namely the number of oscillations of the input s between the thresholds μ and τ.

4 Preisach operator properties

4.1 Preisach plane interpretation

The Preisach hysteresis has an intuitive geometric interpretation, introduced in [33]. Defining the Preisach plane P as in (7), each $(\mu,\tau) \in P$ is identified with a relay hysteron or operator, $\mathcal{R}_{\mu,\tau}$. The weighting function $\rho(\mu,\tau)$ is assumed to have compact support, that is, $\rho(\mu,\tau) = 0$ if $\mu < \mu_0$ or $\tau > \tau_0$ for some μ_0, τ_0. Hence, the half-plane P is delimited by $-M, M$ and the line $\tau = \mu$, the last being congruent with the bound for the Preisach operator integral in (8) and the damage accumulation rule in (2) and (3). In other words, $\rho(\mu,\tau)$ having compact support entails that everything outside the triangle is zero, which is also congruent with the rainflow matrix representation having zeros below the diagonal as pointed out in Section 2.

At any time instant t, the half-plane P can be divided into two regions defined as

$$P^-(t) := P^-_v(t) = \{(\mu,\tau) \in P \mid \mathcal{R}_{\mu,\tau}(v(t)) = 0\} \tag{11}$$

$$P^+(t) := P^+_v(t) = \{(\mu,\tau) \in P \mid \mathcal{R}_{\mu,\tau}(v(t)) = 1\} \tag{12}$$

such that $P = P^-(t) \cup P^+(t)$.

Inspired on the example in [36], an example of a trajectory evolution in the Preisach plane is depicted on Fig. 2. Assume that at initial time t_0, the input $v(t_0) = v_0 < \mu_0$ such that the output of every hysteron is set to 0, or negatively saturated and thus $P^-(t_0) = P$ and $P^+(t_0) = \emptyset$ as shown in Fig. 2*b*. Subsequently, if the input is monotonically increased to some maximum value at the time instant t_1 with $v(t_1) = v_1$, then the output of $\mathcal{R}_{\mu,\tau}$ will switch to 1 as the input v_1 increases past τ. Hence, the horizontal line $\tau = v_1$ divides the Preisach plane into two sets $P^-(t_1)$ and $P^+(t_1)$ as shown in Fig. 2*c*. If the input is then monotonically decreased at time t_2 with $v(t_2) = v_2$, then the output of $\mathcal{R}_{\mu,\tau}$ becomes 0 again as v_2 goes through μ, which corresponds to the vertical line $\mu = v_2$ observed in Fig. 2*d*. This representation will become important in the following section, where we address the approximation by discretisation.

4.2 Approximation by discretisation

The Preisach operator in (8) could be thought as a weighted superposition of all possible relay hysterons, thus the Preisach operator in (8) can be discretised or

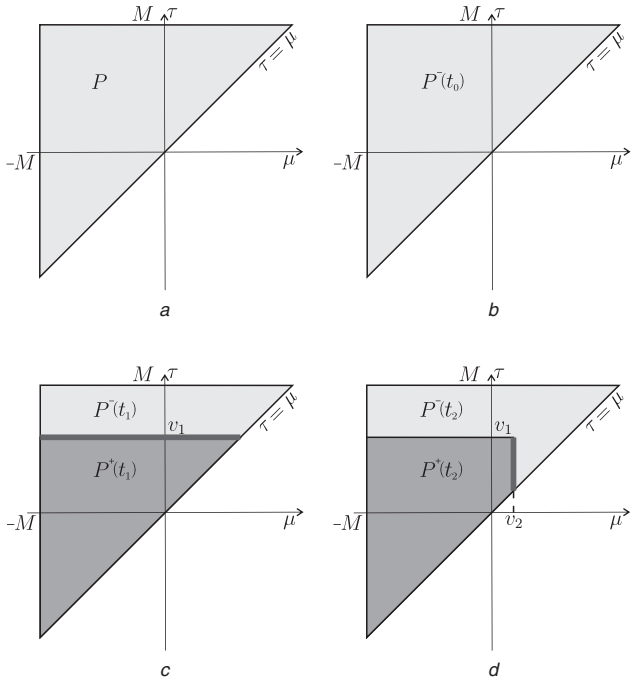

Fig. 2 *Geometric interpretation of the Preisach hysteresis and memory curve*

a P
b P at t_0
c P at t_1
d P at t_2

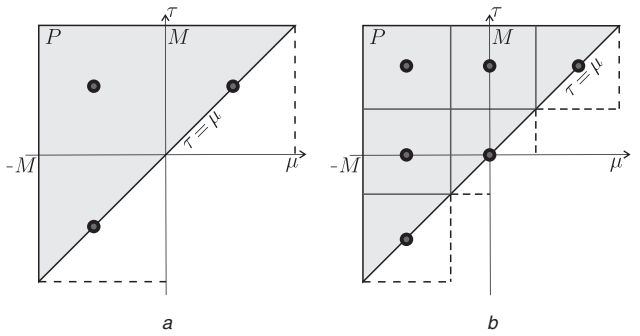

Fig. 3 *Discretisation of the Preisach plane with*

a $L = 2$
b $L = 3$

approximated by a weighted sum of relay hysterons, $\mathcal{H} = \sum_i \nu(\mu_i, \tau_i)\mathcal{R}_{\mu_i,\tau_i}$, for $i \in \mathbb{N}$. As described on [36], its discretisation results in a weighted sum of $L(L+1)/2$ relays, where L is called the discretisation level, and every relay has an individual weighting factor $\nu(\mu_i, \tau_i)$. Fig. 3 shows the Preisach plane for two cases of discretisation: (a) with $L = 2$, corresponding to 3 relays and (b) with $L = 3$, giving rise to 6 relays. This corresponds to a uniform discretisation, dividing the Preisach plane in cells, where each relay is represented as a blue circle at every cell centre in Fig. 3.

4.3 Preisach density function

In order to use the Preisach operator, its density or weighting function $\rho(\mu, \tau)$ needs to be known in general. An identification procedure and a summary of other identification methods can be found in [37], within the context of smart actuators. As addressed in [38], it is also possible to obtain this density function through estimation techniques, for the case of linear systems preceded by Preisach hysteresis. Moreover, while discretising the Preisach operator as mentioned above, the density function $\rho(\mu, \tau)$ is captured by the weightings on each relay $\nu(\mu_i, \tau_i)$. In other words, the density function ρ, might be thought as a gain that changes with the different values of μ and τ.

5 Wind turbine plant model

In the present work, wind generation will be approached from a wind turbine level. The plant model $\mathcal{P}$ to be used, is based on the standard NREL 5MW wind turbine [39]. We will lean on the NREL 5MW wind turbine since it makes comparison with other solutions possible, making it thus a de facto benchmark.

5.1 Wind turbine model

The wind turbine model to be used for simulation assumes that the gearbox is perfectly stiff, while transferring deformations on a low-speed shaft. The low-speed shaft is modelled by a rotational moment of inertia, and a viscously damped rotational spring. The inertia J_r represents the inertia of the rotor and the shaft. Stiffness and damping of the drive train are combined into one spring and one damper on the rotor side with coefficients K_θ and B_θ, respectively. The rotational moment of inertia in the generator side, J_g, represents the collective inertias of the high-speed shaft, gearbox and rotor of the generator. In this model, θ stands for the shaft torsion, ω_g corresponds to the generator angular velocity and ω_r corresponds to the rotor angular velocity.

Fig. 4 shows the structural model of such transmission system. From this model, the following set of differential equations are derived

$$J_r\dot{\omega}_r = T_r - K_\theta\theta - B_\theta\dot{\theta} \tag{13}$$

$$J_g\dot{\omega}_g = -T_g + \frac{K_\theta}{N_g}\theta + \frac{B_\theta}{N_g}\dot{\theta} \tag{14}$$

$$\dot{\theta} = \omega_r - \frac{\omega_g}{N_g} \tag{15}$$

where T_r is the aerodynamic torque, T_g is the generator torque and N_g is the gear ratio.

In addition, the aerodynamic torque of the rotor T_r is given by

$$T_r(\beta, v_r, \omega_r) = \frac{\pi}{2}\rho_a R_r^2 \frac{{v_r}^3}{\omega_r} C_P(\lambda(\omega_r, v_r), \beta) \tag{16}$$

where R_r is the radius of the rotor, ρ_a is the air density, v_r is the effective wind speed and C_P represents the aerodynamic

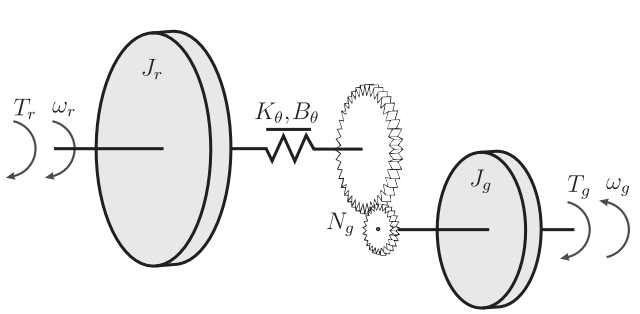

Fig. 4 *Mechanical schematic of the wind turbine transmission system*

doi: 10.1049/iet-cta.2014.0730

efficiency in terms of the collective blade pitch angle β and the tip speed ratio λ is a rational function defined as

$$\lambda(\omega_r, v_r) := \frac{R_r \omega_r}{v_r} \tag{17}$$

Thrust force will be transferred to the tower top through the nacelle, resulting in tower fore-aft motion. It is possible to simplify the tower fore-aft dynamics by the second-order differential equation

$$M_t \ddot{y} + B_t \dot{y} + K_t y = F_t \tag{18}$$

with y being the tower top displacement and M_t, B_t and K_t being the identified mass, damping and stiffness of the model; lastly F_t is the thrust force in the rotor given by

$$F_t(\beta, v_r, \omega_r) = \frac{\pi}{2} \rho_a R_r^2 v_r^2 C_T(\lambda(\omega_r, v_r), \beta) \tag{19}$$

where C_T represents the thrust coefficient in terms of the collective blade pitch angle β and the tip speed ratio λ. In the simulation model, the functions $C_P(\lambda, \beta)$ and $C_T(\lambda, \beta)$ are implemented as look-up tables. Lastly, the electrical power output of the wind turbine will be given by

$$P_{out} = \eta_g \omega_g T_g \tag{20}$$

where η_g is the generator efficiency.

5.2 Linearisation

For the controller design, we take $\boldsymbol{x} = (\omega_g, \omega_r, \theta)$ as the vector of states, $\boldsymbol{u} = (\beta, T_g)$ as the vector of the control inputs and the average ambient wind speed on the rotor area as a disturbance, that is, $\boldsymbol{d} = v_r$. Linearising (13)–(16) around a specific operating point $(\boldsymbol{x}^*, \boldsymbol{u}^*, \boldsymbol{d}^*)$, the following equation is obtained

$$\dot{\bar{\boldsymbol{x}}} = \boldsymbol{A}\bar{\boldsymbol{x}} + \boldsymbol{B}\bar{\boldsymbol{u}} + \boldsymbol{E}\bar{\boldsymbol{d}} \tag{21}$$

where the deviation variables with respect to the chosen operating point are taken as $\bar{\boldsymbol{x}} = \boldsymbol{x} - \boldsymbol{x}^*$, $\bar{\boldsymbol{u}} = \boldsymbol{u} - \boldsymbol{u}^*$ and $\bar{\boldsymbol{d}} = \boldsymbol{d} - \boldsymbol{d}^*$. Consequently, after the linearisation the state equation in (21) in matrix form becomes

$$\dot{\bar{\boldsymbol{x}}} = \begin{bmatrix} -\frac{B_\theta}{J_g N_g^2} & \frac{B_\theta}{J_g N_g} & \frac{K_\theta}{J_g N_g} \\ \frac{B_\theta}{J_r N_g} & \frac{\phi_3 - B_\theta}{J_r} & -\frac{K_\theta}{J_r} \\ -\frac{1}{N_g} & 1 & 0 \end{bmatrix} \bar{\boldsymbol{x}} + \begin{bmatrix} 0 & -\frac{1}{J_g} \\ \frac{\phi_1}{J_r} & 0 \\ 0 & 0 \end{bmatrix} \bar{\boldsymbol{u}} + \begin{bmatrix} 0 \\ \frac{\phi_2}{J_r} \\ 0 \end{bmatrix} \bar{\boldsymbol{d}} \tag{22}$$

where the values of ϕ_1, ϕ_2 and ϕ_3 come from linearising the aerodynamic torque of the rotor T_r in (16) by taking

$$\begin{aligned} T_r(\beta, v_r, \omega_r) &= T_r^* + \left.\frac{\partial T_r}{\partial \beta}\right|_* \bar{\beta} + \left.\frac{\partial T_r}{\partial v_r}\right|_* \bar{v}_r + \left.\frac{\partial T_r}{\partial \omega_r}\right|_* \bar{\omega}_r \\ &\quad + O(\bar{\beta}^2, \bar{v}_r^2, \bar{\omega}_r{}^2) \\ &= T_r^* + \phi_1 \bar{\beta} + \phi_2 \bar{v}_r + \phi_3 \bar{\omega}_r + O(\bar{\beta}^2, \bar{v}_r^2, \bar{\omega}_r{}^2) \end{aligned} \tag{23}$$

In the sequel, we will take $\boldsymbol{x}_k$, $\boldsymbol{u}_k$ and $\boldsymbol{d}_k$ as the discretised versions of $\bar{\boldsymbol{x}}$, $\bar{\boldsymbol{u}}$ and $\bar{\boldsymbol{d}}$ in (21), respectively, such that the discretised linearised dynamics are given as

$$\boldsymbol{x}_{k+1} = \boldsymbol{A}_d \boldsymbol{x}_k + \boldsymbol{B}_d \boldsymbol{u}_k + \boldsymbol{E}_d \boldsymbol{d}_k \tag{24}$$

6 Fatigue reduction MPC strategy

6.1 Control problem formulation

In the baseline MPC strategy $\mathcal{C}_B$, the following optimisation problem is solved

Problem 6 (baseline MPC strategy):

$$\min_{\boldsymbol{U}} \; J = \sum_{k=0}^{N_p-1} \boldsymbol{x}_k^\top \boldsymbol{Q} \boldsymbol{x}_k + \sum_{k=0}^{N_u-1} \boldsymbol{u}_k^\top \boldsymbol{R} \boldsymbol{u}_k + \boldsymbol{x}_{N_p}^\top \boldsymbol{Q}_t \boldsymbol{x}_{N_p} + \boldsymbol{u}_{N_u}^\top \boldsymbol{R}_t \boldsymbol{u}_{N_u}$$

$$s.t. \begin{cases} \boldsymbol{x}_0 = \boldsymbol{x}(t) - \boldsymbol{x}^* \\ \boldsymbol{x}_{k+1} = \boldsymbol{A}_d \boldsymbol{x}_k + \boldsymbol{B}_d \boldsymbol{u}_k, \;\; \text{for } k = 0, \ldots, N_p - 1 \\ \boldsymbol{u}_k = \boldsymbol{u}_{N_u}, \;\; \text{for } N_u + 1 < k < N_p - 1 \end{cases} \tag{25}$$

over $\boldsymbol{U} := \{\boldsymbol{u}_0, \ldots, \boldsymbol{u}_{N_u}\}$ for a prediction horizon $N_p \in \mathbb{N}$ and a control horizon of $N_u \in \mathbb{N}$ time steps, such that $N_p > N_u$, where the problem is subject to the system dynamics. The running cost on states and inputs is given by some weighting matrices $\boldsymbol{Q} = \boldsymbol{Q}^\top \succ 0$, $\boldsymbol{R} = \boldsymbol{R}^\top \succ 0$ and $\boldsymbol{Q}_t = \boldsymbol{Q}_t^\top \succ 0$, $\boldsymbol{R}_t = \boldsymbol{R}_t^\top \succ 0$ are used to weight the terminal cost (see [40, 41]).

The main idea is to control a wind turbine $\mathcal{P}$ reducing both output power fluctuations and the incurred fatigue, see [6, 7]. Nevertheless, the damage estimate is given by a hysteretic element $\mathcal{H}$, namely a discretised Preisach operator, which needs to be incorporated into the MPC strategy. This will be discussed in the following.

6.2 Parameter identification for damage calculation

As previously explained, the general idea is to control a wind turbine $\mathcal{P}$, while reducing both power fluctuations and the incurred fatigue. However, inclusion of the fatigue reduction in (25) is not so straightforward, because of the non-linearity and memory of the hysteresis operator used in the damage calculation. Therefore, the control scheme depicted in Fig. 5*a* is proposed , such that the MPC strategy will be given some parameters a and g, effectively transporting the fatigue calculation to the estimator $\mathcal{K}$.

For the fatigue estimator $\mathcal{K}$, we propose an identification scheme with the shaft torsion $\theta : [0, T] \to \mathbb{R}$ as an input, as depicted on Fig. 5*b*, where $\mathcal{F}$ represents a fatigue estimator in the least squares sense, written as

$$\mathcal{F}(\theta, \dot{\theta}) = a\theta^2 + g\dot{\theta}^2 \tag{26}$$

which is compatible with the MPC formalism, and using the substitution $\alpha \equiv \theta^2$ and $\gamma \equiv \dot{\theta}^2$, we define $\tilde{\mathcal{F}} : \mathbb{R}^2 \to \mathbb{R}$, $(\alpha, \gamma) \mapsto \tilde{\mathcal{F}}(\alpha, \gamma)$, where

$$\tilde{\mathcal{F}}(\alpha, \gamma) = \begin{bmatrix} a & g \end{bmatrix} \begin{bmatrix} \alpha & \gamma \end{bmatrix}^\top \tag{27}$$

with a and g being positive coefficients. The goal of the estimation scheme is to approximate the accumulated damage given by a discretised Preisach operator that provides

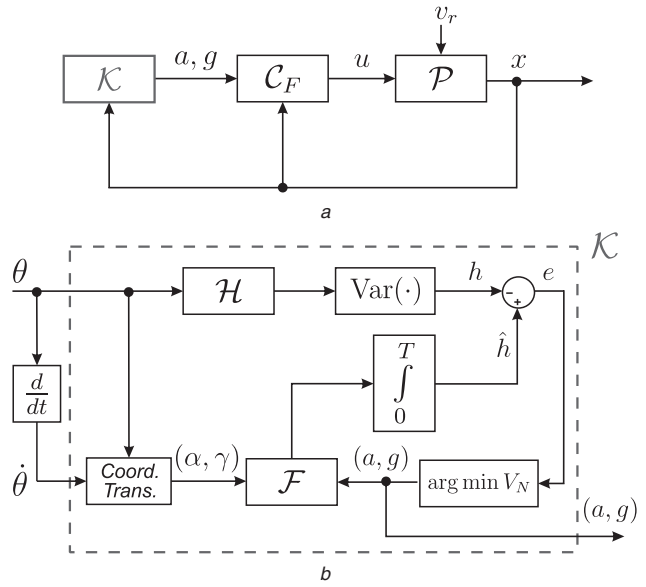

Fig. 5 *Proposed fatigue reduction control strategy*
a MPC scheme with fatigue estimation
b Estimator $\mathcal{K}$: automatic tuning of gains according to fatigue

the damage in the shaft, that is

$$h(\theta) := \mathrm{Var}(\mathcal{H}(\theta)) \tag{28}$$

which is an implementation of the equivalence described in (9). To this end we will construct the estimate

$$\hat{h}(\alpha, \gamma) := \int_0^T \tilde{\mathcal{F}}(\alpha, \gamma)\, \mathrm{d}t \tag{29}$$

In the sequel, we will focus on the discrete realisation of $\tilde{\mathcal{F}}(\alpha, \gamma)$, such that the error $e(k) = h(k) - \hat{h}(k)$ is minimised in the least squares sense according to the criterion

$$V_N(a, g) = \frac{1}{N} \sum_{k=1}^{N} \left\| h(k) - \hat{h}(k) \right\|^2 \tag{30}$$

The estimation of the parameters a and g in the least squares sense will be carried out using an ARX model [42] for a dynamical system with one output, that is, h, and two inputs, viz., α and γ. The ARX model was chosen because of its simplicity, the small number of parameters to be estimated, and the fact that it is consistent with the MPC formalism. Therefore we will use the ARX model

$$\bar{\boldsymbol{A}}(q^{-1})h(k) = \bar{\boldsymbol{B}}(q^{-1}) \begin{bmatrix} \alpha(k) & \gamma(k) \end{bmatrix}^\top + e(k) \tag{31}$$

where q^{-1} is the backward shift operator: $q^{-1}h(k) = h(k-1)$, $\bar{\boldsymbol{B}}(q^{-1}) = \begin{bmatrix} a & g \end{bmatrix} q^0$ gives the desired coefficients a and g, and $\bar{\boldsymbol{A}}(q^{-1}) = 1 + \zeta q^{-1}$ with $\zeta \equiv -1$, accounts for the embedded integrator in $\hat{h}$.

As a result, the fatigue estimator $\mathcal{K}$ will provide the coefficients a and g to the MPC controller $\mathcal{C}_\mathrm{F}$, effectively using a data-based technique to do so; the handling of these parameters by the controller will be addressed in the sequel. An interpretation of this approach is that not only the variance of the torsion is considered, but also the variance of its velocity. This ansatz will be evaluated in the sequel, which is equivalent to approximate h by the variance of the torsion given by the 0th spectral moment, and the variance of the torsion first derivative given by the 2nd spectral moment; this is related to the spectral moments approach taken in [8].

6.3 Redefinition of the cost functional

In order to incorporate the damage estimate into the MPC strategy, the cost functional in (25) needs to be redefined. Thus, we propose the augmented cost functional

$$\bar{J} = J + \tilde{\mathcal{F}}(\alpha_k, \gamma_k) = J + \mathcal{F}(\theta_k, \dot{\theta}_k) \tag{32}$$

where J comes from the baseline MPC, and we redefine the running cost on the states as $\tilde{\boldsymbol{Q}}(a, g) := \boldsymbol{Q} + \bar{\boldsymbol{Q}}(a, g)$, with $\boldsymbol{Q}$ coming from the original problem formulation and $\bar{\boldsymbol{Q}}$ as a function of the parameters a and g provided by the identification by least squares. In order to calculate the extra penalty $\bar{\boldsymbol{Q}}$, we substitute (15) into (26) such that

$$\begin{aligned} \mathcal{F}(\theta, \dot{\theta}) &= a\theta^2 + g\left(\omega_\mathrm{r} - \frac{\omega_\mathrm{g}}{N_\mathrm{g}}\right)^2 \\ &= a\theta^2 + g\omega_\mathrm{r}^2 - 2g\omega_\mathrm{r}\frac{\omega_\mathrm{g}}{N_\mathrm{g}} + g\frac{\omega_\mathrm{g}^2}{N_\mathrm{g}^2} \end{aligned} \tag{33}$$

from which we can obtain the entries of $\bar{\boldsymbol{Q}} \equiv \left[\bar{q}_{ij}\right]$: $\bar{q}_{11} = g/N_\mathrm{g}^2$, $\bar{q}_{22} = g$, $\bar{q}_{33} = a$, $\bar{q}_{12} = \bar{q}_{21} = -g/N_\mathrm{g}$ and $\bar{q}_{23} = \bar{q}_{32} = \bar{q}_{13} = \bar{q}_{31} = 0$. To lean upon convex optimisation, $\bar{\boldsymbol{Q}}$ should be positive semi-definite. By Schur complement, since

$$\boldsymbol{\Psi} := \begin{bmatrix} \bar{q}_{11} & \bar{q}_{12} \\ \bar{q}_{21} & \bar{q}_{22} \end{bmatrix} \succeq 0 \tag{34}$$

then

$$\bar{\boldsymbol{Q}} = \begin{bmatrix} \Psi & 0 \\ 0 & \bar{q}_{33} \end{bmatrix} \succeq 0 \tag{35}$$

for a and g positive; and on account of $\boldsymbol{Q} \succ 0$ by design, we conclude that $\tilde{\boldsymbol{Q}}(a, g) \succeq 0$.

Consequently, the proposed data-based fatigue reduction control strategy $\mathcal{C}_\mathrm{F}$ can be formulated as follows:

Problem 7 (fatigue reduction MPC strategy):

$$\begin{aligned} \min_{\boldsymbol{U}} \; J = &\sum_{k=0}^{N_p-1} \boldsymbol{x}_k^\top \tilde{\boldsymbol{Q}}(a, g)\boldsymbol{x}_k + \sum_{k=0}^{N_u-1} \boldsymbol{u}_k^\top \boldsymbol{R}\boldsymbol{u}_k \\ &+ \boldsymbol{x}_{N_p}^\top \boldsymbol{Q}_\mathrm{t}\boldsymbol{x}_{N_p} + \boldsymbol{u}_{N_u}^\top \boldsymbol{R}_\mathrm{t}\boldsymbol{u}_{N_u} \\ s.t. \; &\begin{cases} \boldsymbol{x}_0 = \boldsymbol{x}(t) - \boldsymbol{x}^* \\ \boldsymbol{x}_{k+1} = \boldsymbol{A}_d\boldsymbol{x}_k + \boldsymbol{B}_d\boldsymbol{u}_k, \;\text{for } k = 0, \ldots, N_p - 1 \\ \boldsymbol{u}_k = \boldsymbol{u}_{N_u}, \;\text{for } N_u + 1 < k < N_p - 1 \end{cases} \end{aligned} \tag{36}$$

over $\boldsymbol{U}$ for a prediction horizon N_p and a control horizon N_u, such that $N_p > N_u$ and weighting matrices $\tilde{\boldsymbol{Q}}(a, g) = \tilde{\boldsymbol{Q}}(a, g)^\top \succeq 0$ and $\boldsymbol{R} = \boldsymbol{R}^\top \succ 0$ on the running cost, and $\boldsymbol{Q}_\mathrm{t} = \boldsymbol{Q}_\mathrm{t}^\top \succ 0$, $\boldsymbol{R}_\mathrm{t} = \boldsymbol{R}_\mathrm{t}^\top \succ 0$ on the terminal cost.

7 Simulation results

The proposed fatigue damage reduction MPC strategy for wind turbines was implemented in `Matlab`. The wind turbine model $\mathcal{P}$ to be controlled is a non-linear model based on the standard NREL 5MW wind turbine [39] implemented

doi: 10.1049/iet-cta.2014.0730

in Simulink, driven to the operating point at a mean wind speed of 18 m/s. The plant model considers the tower dynamics and aerodynamics, as well as the rotational mode of the shaft used for controller design. The parameters for the model in (13)–(16) were also taken from [39]. The controller was synthesised using CVX [43], considering the linearised dynamics in (22) and discretising them with a sampling time of $T_s = 0.15$ s. The control and prediction horizons were set to $N_u = 10$ and $N_p = 20$, respectively, and the simulation was performed for 600 s. The weightings on the running cost were chosen as $\boldsymbol{Q} = \boldsymbol{I}_3$, $\boldsymbol{R} = 1.1\boldsymbol{I}_3$ and the weightings on the terminal costs as $\boldsymbol{Q}_t = 100\boldsymbol{I}_3$ and $\boldsymbol{R}_t = 100\boldsymbol{I}_3$. The wind disturbance $\boldsymbol{d} = v_r$ was taken from wind series data.

The Preisach operator was approximated as a parallel connection of three relay operators, that is, $\mathcal{H}$ with discretisation level $L = 2$, and the thresholds were set to $(\mu_1, \tau_1) = (-0.05M, 0.05M)$, $(\mu_2, \tau_2) = (0.05M, 0.05M)$ and $(\mu_3, \tau_3) = (-0.05M, -0.05M)$, where M is the bound for the Preisach plane calculated as $M = \max\{\min\{\theta\}, \max\{\theta\}\}$; the initial conditions of the relays were given according to

$$w_{-1}(\mu_i, \tau_i) = \begin{cases} 1, & \mu_i + \tau_i < 0 \\ 0, & \mu_i + \tau_i \geq 0 \end{cases} \tag{37}$$

for $i = \{1, 2, 3\}$. The relay weightings were chosen as $\nu_1 = \sigma$, $\nu_2 = \sigma^2$, $\nu_3 = \sigma^3$ for $\nu_1 + \nu_2 + \nu_3 = 1$.

The estimation scheme for $\bar{\boldsymbol{Q}}$ was implemented recursively starting after $t = 3$ s, such that the algorithm has enough data points to calculate an initial estimate of the damage curve. The estimated coefficients a and g are shown in the bottom of Fig. 8, where it can be confirmed that both are positive. In addition, it can be observed that the parameters do not converge to a constant value, but they vary very slowly, adapting to the changes in the damage.

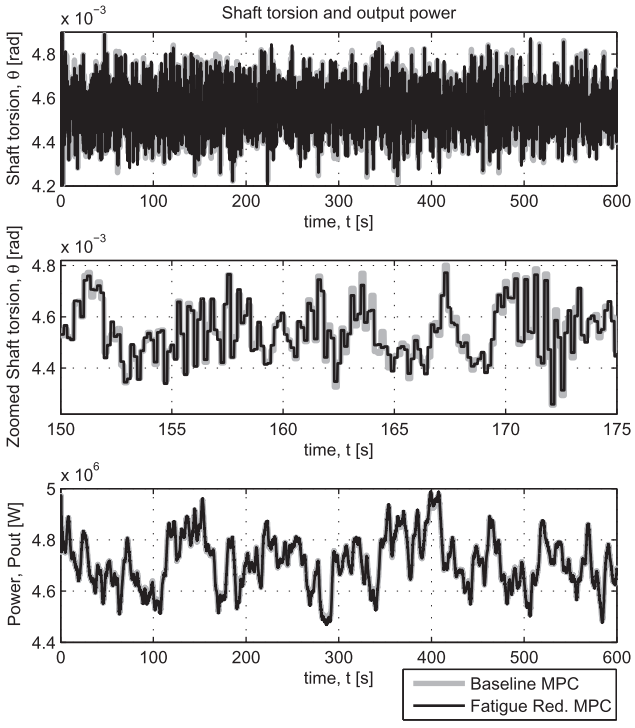

Fig. 6 *Shaft torsion and output power for the baseline and fatigue reduction MPC strategies*

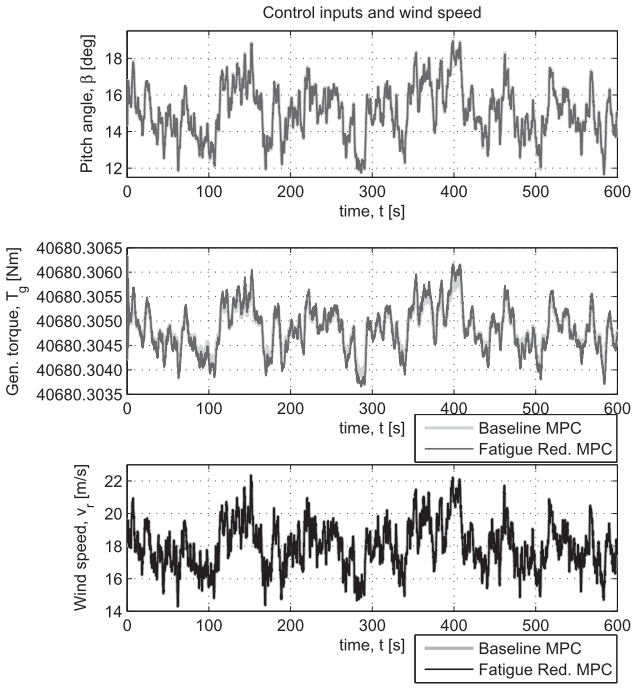

Fig. 7 *Control inputs and disturbance for the baseline and fatigue reduction MPC strategies*

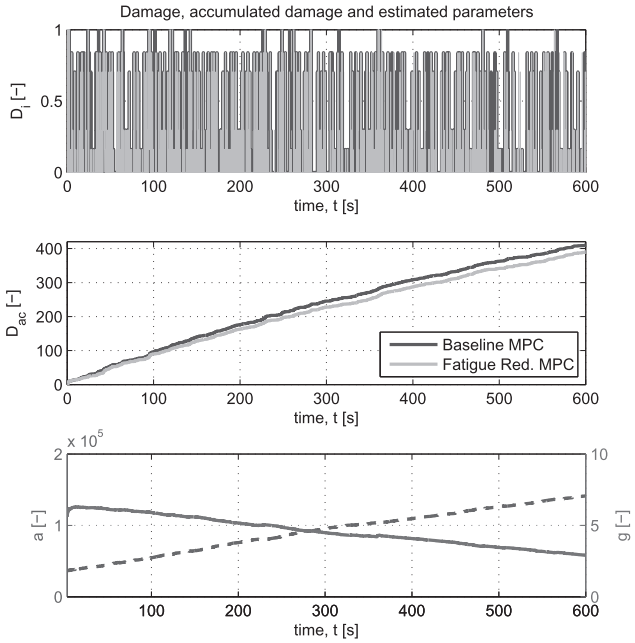

Fig. 8 *Damage estimation in the shaft for $\mathcal{C}_B$ and $\mathcal{C}_F$; and estimated coefficients a (dashed) and g (solid) for $\mathcal{C}_F$*

The shaft torsion and output power, and inputs are shown in Figs. 6 and 7, respectively, for both a baseline MPC strategy $\mathcal{C}_B$ and the fatigue reduction MPC strategy $\mathcal{C}_F$. In Fig. 6, it can be appreciated that both strategies effectively reduce the deviations in both signals, while still showing some sensitivity to the wind. It is worth mentioning that the output power does not decrease with the proposed control strategy $\mathcal{C}_F$, as it can be observed in the bottom of Fig 6. In addition, a zoomed version of the shaft torsion is presented, where it can be observed that the proposed strategy $\mathcal{C}_F$ keeps the oscillations in the shaft torsion within certain bounds, to prevent

some of the damage from occurring. Furthermore, in Fig. 8, the fatigue estimation comparison is shown, where it can be observed that the proposed load reduction MPC strategy effectively achieves a 5% accumulated damage reduction with respect to the baseline strategy $\mathcal{C}_B$. Hence, the proposed control strategy $\mathcal{C}_F$ prevents some damage from occurring by reducing the oscillations in the shaft torsion.

In order to test the effectiveness of the proposed strategy $\mathcal{C}_F$, it was compared against the baseline strategy $\mathcal{C}_B$ in the context of equivalent damage loads. Consequently, the shaft torsion θ for both cases was run through NREL's `MCrunch` post-processor for wind turbine data analysis [44]. Comparing the outcome, the proposed method achieves a damage reduction of 4.27% compared against the baseline strategy, thanks to the gains a and g provided by the fatigue estimator $\mathcal{K}$. The reason for this additional check is that in the process of incorporating the fatigue estimation into the MPC formalism the following assumptions were made: symmetric RFC applies, discretisation of the Preisach operator and fatigue approximation by least squares.

8 Conclusions

Throughout this paper a fatigue damage estimation technique based on Preiscach hysteresis operators was introduced and explained, with the aim to use it in online fatigue estimation for control. Moreover, its relation with the RFC method was also addressed, due to the fact that RFC is the most widely accepted method for the fatigue estimation. The equivalence between RFC and a Preisach operator introduced in [13] provides the opportunity to use the latter for online implementation in control loops. It is worth mentioning that the results in Proposition 5 apply to symmetric RFC, and not all RFC methods are symmetric; for symmetric RFC the so-called Madelung rules apply, that is, deletion pairs commute, meaning that it does not matter how the sequences are deleted. However, in our case the primal concern is to apply this technique online, so no deletion is actually possible.

A fatigue damage reduction data-based MPC strategy was designed and implemented. This strategy was implemented on a non-linear model based on the standard NREL 5MW wind turbine and it was compared against a baseline MPC strategy, achieving damage reduction in the shaft. Perhaps one shortcoming of our approach is the fact that the residual cannot be considered directly, which would require the periodic version of the hysteresis operator, but the contribution of the residual would not be so large if a sufficiently large time window were considered. Other considerations to take into account are the hysteresis free parameters, that is, weighting functions, the thresholds and discretisation level, which could be fitted if the S-N parameters of the material are known, or could be identified.

Finally, it could be argued that linear and continuous identification methods are not enough to capture all the behaviour of the hysteresis operator, because of its non-linear nature, discontinuities and memory effects. Nonetheless, the variation operator introduces a certain regularisation, that is, the integral or accumulation action as shown in the accumulated damage in Fig. 8; this regularisation allows the identification to work and enables the controller to achieve a significant damage reduction. Lastly, the approach presented in this paper, allows a self-tuning data-based MPC strategy to be implemented in real-time control, effectively incorporating the damage of the components into the control problem formulation, via the cost functional. Moreover, this damage estimation and control scheme might prove to be a useful tool for component damage monitoring and maintenance planning, especially for off-shore turbines, where the access is difficult and costly.

9 Acknowledgments

This work was partially supported by the Danish Council for Strategic Research (contract no. 11-116843) within the 'Programme Sustainable Energy and Environment', under the 'EDGE' (Efficient Distribution of Green Energy) research project.

10 References

1 Schütz, W.: 'A history of fatigue', *Eng. Fract. Mech.*, 1996, **54**, (2), pp. 263–300
2 Wöhler, A.: 'Versuche über die Festigkeit der Eisenbahnwagenachsen', *Z. für Bauwesen*, 1860, **10**, pp. 160–161
3 Palmgren, A.: 'Die Lebensdauer von Kugellagern', *Z. des Vereins Deutscher Ingenieure*, 1924, **68**, (14), pp. 339–341
4 Miner, M.A.: 'Cumulative damage in fatigue', *J. Appl. Mech.*, 1945, **12**, (3), pp. 159–164
5 Endo, T., Mitsunaga, K., Nakagawa, H.: 'Fatigue of metals subjected to varying stress-prediction of fatigue lives'. Preliminary Proc. of the Chugoku-Shikoku District Meeting, 1967, pp. 41–44
6 Soltani, M., Wisniewski, R., Brath, P., Boyd, S.: 'Load reduction of wind turbines using receding horizon control'. Proc. IEEE Conf. Control Applications (CCA), 2011, pp. 852–857
7 Mirzaei, M., Soltani, M., Poulsen, N.K., Niemann, H.H.,: 'Model predictive control of wind turbines using uncertain LIDAR measurements'. Proc. American Control Conf. (ACC), 2013, pp. 2235–2240
8 Hammerum, K., Brath, P., Poulsen, N.K.: 'A fatigue approach to wind turbine control', *J. Phys., Conf. Ser.*, 2007, **75**, (1), p. 012081
9 Bossanyi, E.A.: 'Wind turbine control for load reduction', *Wind Energy*, 2003, **6**, (3), pp. 229–244
10 Bossanyi, E.A.: 'Further load reductions with individual pitch control', *Wind Energy*, 2005, **8**, (4), pp. 481–485
11 Larsen, T.J., Madsen, H.A., Thomsen, K.: 'Active load reduction using individual pitch, based on local blade flow measurements', *Wind Energy*, 2005, **8**, (1), pp. 67–80
12 Soleimanzadeh, M., Wisniewski, R.: 'Controller design for a wind farm, considering both power and load aspects', *Mechatronics*, 2011, **21**, (4), pp. 720–727
13 Brokate, M., Dreßler, K., Krejčí, P.: 'Rainflow counting and energy dissipation for hysteresis models in elastoplasticity', *Eur. J. Mech. A, Solids*, 1996, **15**, (4), pp. 705–737
14 Brokate, M.: 'Optimale Steuerung von gewöhnlichen Differentialgleichungen mit Nichtlinearitäten vom Hysteresis-Typ', (P. Lang, 1987), vol. 35
15 Belbas, S.A., Mayergoyz, I.D.: 'Dynamic programming for systems with hysteresis', *Phys. B, Condens. Matter*, 2001, **306**, (1), pp. 200–205
16 Belbas, S.A., Mayergoyz, I.D.: 'Optimal control of dynamical systems with Preisach hysteresis', *Int. J. Non-linear Mech.*, 2002, **37**, (8), pp. 1351–1361
17 Bagagiolo, F.: 'An infinite horizon optimal control problem for some switching systems', *Discrete Continuous Dyn. Sys., B*, 2001, **1**, pp. 443–462
18 Bagagiolo, F.: 'Viscosity solutions for an optimal control problem with Preisach hysteresis nonlinearities', *ESAIM, Control, Optimisation Calc. Var.*, 2004, **10**, (2), pp. 271–294
19 Hjalmarsson, H., Gevers, M., Gunnarsson, S., Lequin, O.: 'Iterative feedback tuning: theory and applications', *IEEE Control Syst.*, 1998, **18**, (4), pp. 26–41
20 Yin, S,. Li, Xi., Gao, H., Kaynak, O.: 'Data-based techniques focused on modern industry: an overview', *IEEE Trans. Ind. Electron.*, 2014, (61), **11**, 6418–6438
21 Yin, S., Ding, S., Xie, X., Luo, H.: 'A review on basic data-driven approaches for industrial process monitoring', *IEEE Trans. Ind. Electron.*, 2014, **61**, (11), pp. 6418–6428
22 Yin, S., Wang, G., Karimi, H.R.: 'Data-driven design of robust fault detection system for wind turbines', *Mechatronics*, 2014, **24**, (4), pp. 298–306
23 Yin, S., Yang, X., Karimi, H.R.: 'Data-driven adaptive observer for fault diagnosis', *Math. Probl. Eng.*, 2012, **2012**

doi: 10.1049/iet-cta.2014.0730

24 Yin, S., Wang, G., Yang, X.: 'Robust PLS approach for KPI-related prediction and diagnosis against outliers and missing data', *Int. J. Syst. Sci.*, 2014, **45**, (7), pp. 1375–1382
25 Johannesson, P.: 'Rainflow analysis of switching Markov loads'. PhD thesis, Lund University, 1999
26 Downing, S.D., Socie, D.F.: 'Simple rainflow counting algorithms', *Int. J. Fatigue*, 1982, **4**, (1), pp. 31–40
27 Rychlik, I.: 'A new definition of the rainflow cycle counting method', *Int. J. Fatigue*, 1987, **9**, (2), pp. 119–121
28 Niesłony, A.: 'Determination of fragments of multiaxial service loading strongly influencing the fatigue of machine components', *Mech. Syst. Signal Process.*, 2009, **23**, (8), pp. 2712–2721
29 Sobczyk, K.: 'Stochastic models for fatigue damage of materials', *Adv. Appl. Probab.*, 1987, **19**, 652–673
30 Bishop, N.W.M.: 'Vibration fatigue analysis in the finite element environment'. XVI Encuentro Del Grupo Español De Fractura, Spain, 1999
31 Tchankov, D.S., Vesselinov, K.V.: 'Fatigue life prediction under random loading using total hysteresis energy', *Int. J. Press. Vessels Pip.*, 1998, **75**, (13), pp. 955–960
32 Krasnosel'skiĭ, M.A., Pokrovskiĭ, A.V.: 'Systems with hysteresis' (Springer Verlag, 1989)
33 Mayergoyz, I.D.: 'Mathematical models of hysteresis' (Springer Verlag, 1991)
34 Brokate, M., Sprekels, J.: 'Hysteresis and phase transitions' (Springer Verlag, Applied Mathematical Sciences, 1996), vol. 121
35 Preisach, F.: 'Über die Magnetische Nachwirkung', *Z. für Phys.*, 1935, **94**, (5–6), pp. 277–302
36 Tan, X., Baras, J.S., Krishnaprasad, P.S.: 'Control of hysteresis in smart actuators with application to micro-positioning', *Syst. Control Lett.*, 2005, **54**, (5), pp. 483–492
37 Tan, X., Venkataraman, R., Krishnaprasad, P.S.: 'Control of hysteresis: theory and experimental results', *Proc. SPIE*, 2001, **4326**, pp. 101–112
38 Chen, X.: 'Control for unknown linear systems preceded by hysteresis Represented by Preisach model'. Proc. IEEE Conf. Decision and Control (CDC), 2013, pp. 6664–6669
39 Jonkman, J.M., Butterfield, S., Musial, W., Scott, G.: 'Definition of a 5-MW reference wind turbine for offshore system development'. National Renewable Energy Laboratory Colorado, 2009
40 Maciejowski, J.M., Huzmezan, M.: 'Predictive control with constraints' (Springer, 1997)
41 Camacho, E.F., Bordons, C.: 'Model predictive control', (Springer, London, 2004)
42 Ljung, L.: 'System identification: theory for the user' (Prentice-Hall, 1987)
43 Grant, M., Boyd, S.: 'CVX: Matlab software for disciplined convex programming, version 2.1', http://www.cvxr.com/cvx, 2014
44 Buhl, M.L.: 'MCrunch user's guide for vrsion 1.00', National Renewable Energy Laboratory, 2008

11 Appendix: Damage calculation with periodic operators

The damage estimate provided in (2) does not evaluate the contribution of the residual $s_{\mathcal{M}}$ to the total damage; namely, when the counting algorithm stops, being referred to as the rainflow residual of s. The contribution of the residual can be taken into account by defining the periodic rainflow count as

$$c_{\text{per}}(s) := c(s) + c(s_{\mathcal{M}}, s_{\mathcal{M}}) \tag{38}$$

This is needed to consider a periodic equivalent of the rainflow count, where damage contribution of the irreducible string $s_{\mathcal{M}}$ is considered (for further details refer to [34]).

In [34], the following corollary is presented from which it is concluded that the total damage can be represented as the variation of the output of a suitably chosen hysteresis operator. The intuition behind this is that the RFC is related to counting oscillations corresponding to certain amplitudes, and this behaviour is captured by the number of oscillations of s between certain thresholds.

Definition 8 (periodic relay hysteresis operator): Using the relay operator definition, let its periodic version be defined by

$$\mathcal{R}^{\text{per}}_{\mu,\tau}(s; w_{-1}) := \mathcal{R}_{\mu,\tau}(s; w^{\text{per}}_{-1}), \quad s \in S,\ w_{-1} \in \{0, 1\} \tag{39}$$

where w^{per}_{-1} denotes the last entry of the string $\mathcal{R}_{\mu,\tau}(s; w_{-1})$. In other words

$$\mathcal{R}_{\mu,\tau}(s, s; w_{-1}) = (\mathcal{R}_{\mu,\tau}(s; w_{-1}), \mathcal{R}^{\text{per}}_{\mu,\tau}(s; w_{-1})) \tag{40}$$

The periodic version of the relay operator, $\mathcal{R}^{\text{per}}_{\mu,\tau}(s)$, will be used in Proposition 9 to remove the assumption $w_{-1} = w_0 = w_N$. Therefore, to take into account the residual into the counting, the periodic version of the relay is needed.

Proposition 9 (periodic relay variation): For any $s = (v_0, \ldots, v_N) \in S$ with $v_0 = v_N$ it holds

$$\text{Var}(\mathcal{R}^{\text{per}}_{\mu,\tau}(s; w_{-1})) = 2 \sum_{\xi \le \mu \le \tau \le \eta} c_{\text{per}}(s)(\xi, \eta) \tag{41}$$

for any w_{-1}.

For further details see Proposition 2.9 in [13] or Corollary 2.6.17 in [34] (notice that the relay definition differs in the output value: in [13] $w_i = 0$ for $v_i \le \mu$ and in [34] $w_i = -1$ for $v_i \le \mu$, which affects in turn the number before the sum in (41)). Owing to Proposition 9, the choice of the initial values $w_{-1}(\mu, \tau)$ for the relays $\mathcal{R}_{\mu,\tau}$ does not affect the further results, so it will be assumed that

$$w_{-1}(\mu, \tau) = \begin{cases} 1, & \mu + \tau < 0 \\ 0, & \mu + \tau \ge 0 \end{cases} \tag{42}$$

which was used for the initial values of the relays in Section 7.

Lastly, since the relay operator appears in the definition of the Preisach operator, then by replacing it by its periodic version, a periodic version of the Preisach operator is obtained.